X. H. Zhang[1]
Associate Professor
Institute of Mechanics, CAS,
No. 15 Beisihuanxi Road,
Beijing 100190, China
e-mail: zhangxuhui@imech.ac.cn

X. B. Lu
Institute of Mechanics, CAS,
No. 15 Beisihuanxi Road,
Beijing 100190, China
e-mail: xblu@imech.ac.cn

Z. M. Zheng
Institute of Mechanics, CAS,
No. 15 Beisihuanxi Road,
Beijing 100190, China
e-mail: zhengzm@lnm.imech.ac.cn

L. M. Zhang
Hong Kong University of
Science and Technology,
Clear Water Bay, Hong Kong
e-mail: cezhangl@ust.hk

Heat-Induced Evolution of Phase Transformations in Tetrahydrofuran Hydrate-Bearing Sediment

Heat conduction and phase transformations are basic physical-chemical process and control the kinetics of dissociation, fluid flow and strata deformation during hydrate dissociation in sediments. This paper presents a simplified analysis of the thermal process by assuming that the heat-induced evolution can be decoupled from flow and deformation processes. Self-similar solutions for one-, two- and three-phase transformation fronts are obtained. A series of experiments on THF-hydrate-bearing sediments was conducted to test the theory. The theoretical, numerical and experimental results on the evolution of hydrate dissociation front in the sediment are in good agreement.
[DOI: 10.1115/1.4026454]

Keywords: hydrate-bearing sediment, heat-induced evolution, hydrate dissociation, phase transformation front

1 Introduction

Natural gas hydrate is a crystalline solid composed mainly of methane gas molecules and water molecules. It is stabilized in conditions of high pressure and low temperature. It is conservatively estimated that more than 9.4 terratonnes of organic carbon is present in the form of gas hydrate in ocean sediments, continental margins and deep lakes, and extraction of methane from hydrates could provide a future energy resource [1–4].

Generally, 1 cubic meter of methane gas hydrate releases about 164 cubic meters of methane gas and 0.8 cubic meters of water at 1 atm and a temperature of 0 °C. If the released gas could not drain quickly, excess pore pressure will generate and the strength of hydrate-bearing sediments (HBS) will decrease, which may lead to environmental disasters, geological disasters, destruction of ocean platforms and oil wells, or even gas blowouts [5–13].

Heat transfer leads to the dissociation of gas hydrate and the simultaneous generation of variable stress field with the seepage of pore fluids and the deformation of the soil layer. Accordingly, failure of ocean floor and environmental disasters can occur. The expansion of the hydrate dissociation front due to heat conduction and phase transformations is important for the evaluation of the failures. In the three main rate-limiting factors to gas hydrate dissociation, i.e., Fluid flow, heat transfer and intrinsic kinetics, generally, heat transfer plays a controlling role due to the least time scale [14].

The expansion of a hydrate dissociation zone induced by an oil pipe with a high temperature of 100 °C in HBS was studied based on heat conduction theory [15]. It is shown that the hydrate dissociation front around a high temperature oil pipe 1 m in diameter can reach 20 m in 15 years and 30 m in 40 years, which may cause instability of the pipe. A model was presented to describe the hydrate phase transition [16]. Hydrates are assumed to dissociate instantly and completely once the phase equilibrium condition is satisfied. This creates a dissociation zone and a non-dissociation zone (hydrate stability zone) divided by the dissociation front. Conservation of energy and mass is not fully considered in this case.

Several other analytical and numerical studies on the expansion of hydrate dissociation zone in HBS have been conducted, which coupled kinetic hydrate dissociation, gas or/and water flow, heat conduction and energy conservation [17–20]. By depressurization method in gas hydrate-bearing sediment, the sharp-interface assumption is regarded not valid when seepage and low hydrate saturation are considered [21]. However, analytical solutions are difficult to obtain and the simulation results need to be verified by laboratory or in-situ data.

Tetrahydrofuran (THF) hydrate-bearing sediments are often adopted as a good substitute for methane hydrate in laboratory experiments due to the similarity in mechanical and thermal properties and a large volume of THF sediment can be synthesized more homogeneously, naturally and safely than synthesized methane hydrate sediment, since THF is completely miscible with water in all proportions and forms hydrate at 1 atm and 20 °C [22–26].

A model considering heat conduction and phase transformations during THF hydrate dissociation in sediments is proposed and high temperature (>100 °C) induced THF hydrate dissociation of simplified geometry is considered [27]. The objective of this paper is to further study the heat-induced evolution of hydrate dissociation in hydrate-bearing sediments and provide a detailed analytical method and solution for heat conduction containing hydrate dissociation and multi-phase transformations. First, a self-similar method is presented and an analysis of heat conduction considering one-, two-, and three-phase transformation fronts in sediment is conducted, accompanied by numerical simulations. Following that a one-dimensional apparatus is describes and a series of experiments on THF HBS is presented in which the soil deformation and gas or water seepage can be ignored.

2 Mathematical Model for Evolution of Phase Transformation in HBS

In this paper, phase transformations are assumed to be front-melting processes and the energy and the mass conservation is considered at the fronts. A mathematical model considering

[1]Corresponding author.

Contributed by the Heat Transfer Division of ASME for publication in the Journal of Heat Transfer. Manuscript received June 11, 2012; final manuscript received January 3, 2014; published online March 6, 2014. Assoc. Editor: Wei Tong.

 Copyright © 2014 by ASME

Downloaded From: http://heattransfer.asmedigitalcollection.asme.org/ on 06/19/2014 Terms of Use: http://asme.org/terms

one-, two-, and three-phase transformation fronts is presented in this section.

2.1 Physical Description. The molecular formula of hydrate is noted as $M{\cdot}nH_2O$ (M: Gas molecule or THF molecule; H_2O: Water molecule; and n: Hydrate number). The formation mechanism of the transformation fronts can be described as follows (The effect of seepage is not considered temporarily): First, the temperature of the sediment surrounding a thermal source increases, causing hydrates to dissociate into water and liquid M (liquid THF here). When the phase equilibrium temperature is reached, a hydrate dissociation zone and a non-dissociated zone form and are divided by the dissociation front. Second, the liquid is gasified when the gasification temperature is reached, and so a gasification zone forms and is separated from the hydrate dissociation zone by the gasification front. Finally, water is transformed into vapor when the boiling temperature is reached, and the gasification zone and water vaporization zone are divided by the vaporization front. These three fronts all expand with time. The formation of four zones $Z1$, $Z2$, $Z3$, $Z4$ and three fronts $F1$, $F2$, $F3$ in the hydrate sediment is shown schematically in Fig. 1.

2.2 Governing Equations. In the present model the following assumptions are adopted: (1) The thermodynamic parameters of each phase in each miscible zone are the average values. (2) The enthalpies of water, liquid, and hydrate are constant. Based on the mixture theory, the one-dimensional equation considering the thermal-induced dissociation of hydrate can be referred to theory in heat conduction [28] expressed as

$$C\rho\frac{\partial T}{\partial t}=K\frac{\partial^2 T}{\partial x^2}+\rho_h\Delta H_{h\to w+f}\frac{\partial \varepsilon_h}{\partial t}+\rho_f\Delta H_{f\to fg}\frac{\partial \varepsilon_f}{\partial t}+\rho_w\Delta H_{w\to wg}\frac{\partial \varepsilon_w}{\partial t} \tag{1}$$

in which the thermodynamic parameters in each zone are as follows:

$$\rho C=\varepsilon_w\rho_w C_w+\varepsilon_{wg}\rho_{wg}C_{wg}+\varepsilon_f\rho_f C_f+\varepsilon_{fg}\rho_{fg}C_{fg}+\varepsilon_s\rho_s C_s+\varepsilon_h\rho_h C_h \tag{2}$$

$$K=\varepsilon_w K_w+\varepsilon_{wg}K_{wg}+\varepsilon_f K_f+\varepsilon_{fg}K_{fg}+\varepsilon_s K_s+\varepsilon_h K_h \tag{3}$$

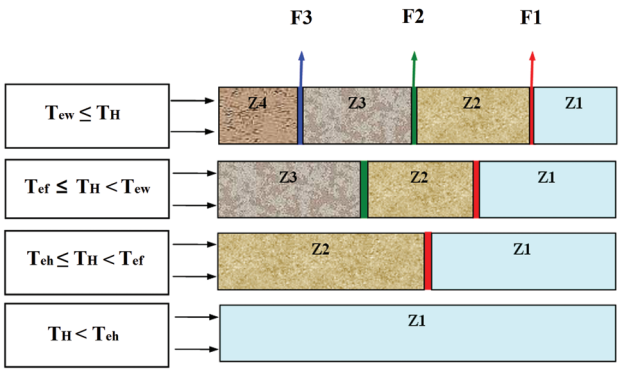

Fig. 1 Evolution of phase transformation fronts. Note: Z1, non-dissociated zone: hydrate and sediment skeleton; Z2, hydrate dissociation zone: liquid, water and sediment skeleton; Z3, gasification zone: gas, water and sediment skeleton; Z4, water vaporization zone: sediment skeleton, water vapor, gas; F1, hydrate dissociation front; F2, gasification front; F3, water vaporization front; T_H and T_{ew}, T_{ef}, T_{eh} represent the heat source temperature and the phase transformation temperatures of water to water vapor, liquid to gas, hydrate dissociation.

It is noted that the thermal conductivity is expressed as average that of each phase which is one of that for some methane hydrate sediments [29–31].

There are two obvious characteristics in crystal phase transformation: One is that the temperature inside the phase transformation zone remains at the phase transformation point. The other is that phase transformation occurs only when the total provided energy is sufficient for crystal phase transformation.

Thus the following two assumptions are adopted:

(1) Phase transformation occurs once both the threshold temperature and the latent heat are satisfied, so the following equations are satisfied:

$$\varepsilon_h=H(x-X_{eh}(t)) \tag{4}$$

$$\varepsilon_f=H(x-X_{ef}(t)) \tag{5}$$

$$\varepsilon_w=H(x-X_{ew}(t)) \tag{6}$$

(2) Temperature is continuous and equal to the phase equilibrium temperature at the phase transformation front, i.e., $T(X_e)=T_e$.

Substituting assumption (1) into Eq. (1) and integrating on both sides of the phase transformation front, we can obtain

$$K\frac{\partial T}{\partial x}\bigg|_{X_{ei}+}-K\frac{\partial T}{\partial x}_{X_{ei}-}=\rho_i\Delta H\varepsilon_i\frac{\mathrm{d}X_{ei}}{\mathrm{d}t} \tag{7}$$

Equation (7) shows the condition of temperature gradient at the phase transformation front and meanwhile indicates the conservation of energy. The index, i here represents phase f, w, h, respectively. The subscript ei indicates the phase transformation status of phase i.

The mathematical model can be written as follows by combining Eq. (1) with Eq. (7) and utilizing the boundary and initial conditions which are similar with multiple Stefan problems [32]

Governing equation:

$$\rho C\frac{\partial T}{\partial t}=K\frac{\partial^2 T}{\partial x^2} \tag{8}$$

Boundary conditions:

$$x=0,\quad T=T_H \text{ and } x=l,\quad T=T_0 \tag{9}$$

Initial conditions:

$$t=0,\quad T=T_0 \tag{10}$$

Joining conditions at the phase transformation fronts:

$$T(X_{ei}(t))=T_{ei} \text{ and } K\frac{\partial T}{\partial x}\bigg|_{X_{ei}+}-K\frac{\partial T}{\partial x}\bigg|_{X_{ei}-}=\rho_i\Delta H\varepsilon_i\frac{\mathrm{d}X_{ei}}{\mathrm{d}t} \tag{11}$$

2.3 Self-Similarity Analysis. For a problem without characteristic dimensions or time, the time variable and the space variable can be combined as one independent variable, and the analytical solution can be obtained easily by a self-similarity analysis.

The dimensions of HBS are assumed as infinite, and so there are no characteristic length and time in this problem. For simplification, the problems of hydrate dissociation front F1 and two zones $Z1$ and $Z2$ are considered here (Fig. 2). For cases involving more zones and phase transformation fronts, the solutions can be obtained in a similar way.

For zone $Z1$, the average density, specific heat, and conductivity can be expressed as follows:

Downloaded From: http://heattransfer.asmedigitalcollection.asme.org/ on 06/19/2014 Terms of Use: http://asme.org/terms

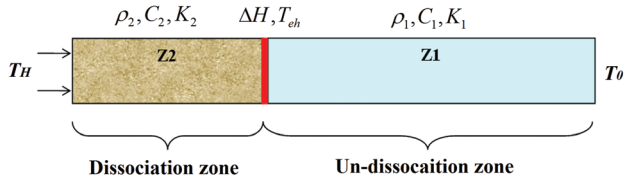

Fig. 2 Division of dissociation and non-dissociated zones

$$\rho_1 = \varepsilon_h \rho_h + \varepsilon_s \rho_s \tag{12}$$

$$C_1 = \varepsilon_h C_h + \varepsilon_s C_s \tag{13}$$

$$K_1 = \varepsilon_h K_h + \varepsilon_s K_s \tag{14}$$

For zone $Z2$, the average density, specific heat, and conductivity can be expressed as follows:

$$\rho_2 = \varepsilon_f \rho_f + \varepsilon_s \rho_s + \varepsilon_w \rho_w \tag{15}$$

$$C_2 = \varepsilon_f C_f + \varepsilon_s C_s + \varepsilon_w C_w \tag{16}$$

$$K_2 = \varepsilon_f K_f + \varepsilon_s K_s + \varepsilon_w K_w \tag{17}$$

At the transformation front, the latent heat of hydrate dissociation is ΔH_h, and the phase transformation temperature is T_{eh}. The porosity of the sediments is ε_0. The temperature evolution with time and space can be written in the following form:

$$T = f(x, t, T_h, T_0, T_e, \rho_1, C_1, K_1, \rho_2, C_2, K_2, \Delta H, \varepsilon_0) \tag{18}$$

The physical process of thermal conduction is that heat transfer is temperature difference driven, which is determined by temperature differences $\theta = T - T_0$ and thermal diffusivities $\kappa = (K/\rho C)$. So Eq. (18) can be rewritten as

$$\theta = f\left(x, t, \kappa_1, \kappa_2, \theta_H, \theta_{eh}, \frac{K_1}{\rho_h \Delta H \varepsilon_0}, \frac{K_2}{\rho_h \Delta H \varepsilon_0}\right) \tag{19}$$

in which $\theta_H = T_H - T_0$ and $\theta_{eh} = T_{eh} - T_0$.

Using the time variable t, the thermal diffusivity κ_1 in zone 1, and the difference between heating temperature and initial temperature θ_H as three basic variables, Eq. (18) can be rewritten as

$$\frac{\theta}{\theta_H} = f\left(\frac{x^2}{\kappa_1 t}, \frac{\kappa_1}{\kappa_2}, \frac{\theta_{eh}}{\theta_H}, \frac{\theta_H K_1}{\kappa_1 \rho_h \Delta H \varepsilon_0}, \frac{\theta_H K_2}{\kappa_1 \rho_h \Delta H \varepsilon_0}\right) \tag{20}$$

in which (κ_1/κ_2), (θ_{eh}/θ_H), $(\theta_H K_1/\kappa_1 \rho_h \Delta H \varepsilon_0)$, and $(\theta_H K_2/\kappa_1 \rho_h \Delta H \varepsilon_0)$ are four controlling parameters.

When the four controlling parameters are constant, substituting $\xi = (x^2/\kappa_1 t)$ and $\vartheta = (\theta/\theta_H)$ into Eq. (20), the following equation can be obtained:

$$\vartheta = f(\xi) \tag{21}$$

Equation (21) illustrates that the evolution of temperature is determined by a variable combining space and time. Figure 3 shows a planar coordinate system (x, t), in which the contour lines of ξ are drawn and each line represents a space evolution of a certain temperature with time; especially $\xi = 0$ and $\xi \to \infty$ represent the locations with temperatures of T_H and T_0, respectively. The contour line ξ_e represents the hydrate dissociation, i.e., the evolution of hydrate dissociation front, which divides the planar system into two zones (Fig. 2). The contour lines of ξ in zones $Z1$ and $Z2$ share the common characteristic heat conduction. So the evolution of the hydrate dissociation and phase transformation fronts are self-similar and the partial differential equation and initial and boundary conditions (8)–(11) for heat conduction considering phase transformations can be simplified into an ordinary differential equation.

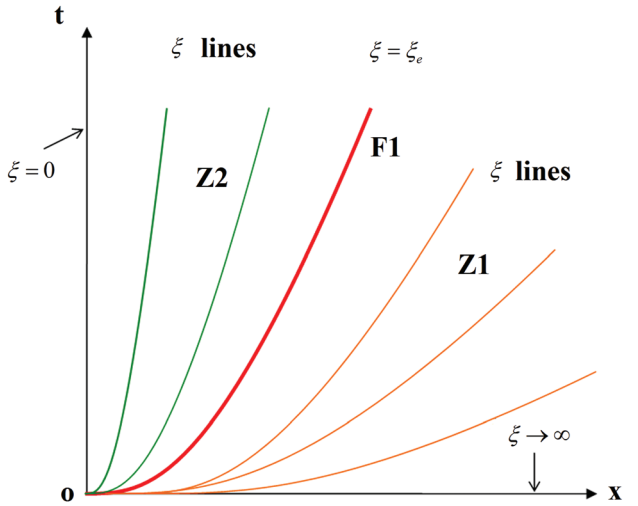

Fig. 3 ξ lines at the hydrate dissociation front F1 and different zones, each line tracks the location of a given temperature with time

Substituting variable $\xi = (x^2/\kappa_1 t)$ into Eq. (8), an ordinary differential equation is obtained

$$4\frac{\mathrm{d}^2\vartheta}{\mathrm{d}\xi^2} + \left(\frac{\kappa_1}{\kappa} + \frac{2}{\xi}\right)\frac{\mathrm{d}\vartheta}{\mathrm{d}\xi} = 0 \tag{22}$$

2.4 Self-Similarity Solutions

2.4.1 One Transformation Front Case. For the problem with one transformation front, the governing equations and boundary conditions in zones $Z1$ and $Z2$ can be rewritten as

In zone Zi (i denote 1 and 2 here):

Governing equation:

$$4\frac{\mathrm{d}^2\vartheta_i}{\mathrm{d}\xi^2} + \left(\frac{\kappa_1}{\kappa_i} + \frac{2}{\xi}\right)\frac{\mathrm{d}\vartheta_i}{\mathrm{d}\xi} = 0 \tag{23}$$

Boundary conditions:

$$\xi = 0 : \vartheta = 1; \xi \to \infty : \vartheta = 0; \quad \xi = \xi_e : \vartheta = \vartheta_e \tag{24}$$

Connecting condition:

$$\xi = \xi_e : \frac{4\theta_H K_1}{\rho_h \Delta H \varepsilon_0 \kappa_1}\frac{\partial \vartheta_1}{\partial \xi} - \frac{4\theta_H K_2}{\rho_h \Delta H \varepsilon_0 \kappa_1}\frac{\partial \vartheta_2}{\partial \xi} = 1 \tag{25}$$

Substituting $\mathrm{erf}(\sqrt{\xi}) = (2/\sqrt{\pi})\int_0^{\sqrt{\xi}} \exp(-\xi^2)\mathrm{d}\xi$ into Eqs. (22)–(25), solutions for each zone are obtained

In zone $Z1$:

$$\vartheta_1 = \frac{\vartheta_e}{\mathrm{erf}\left(\frac{1}{2}\sqrt{\xi_e}\right) - 1} \cdot \mathrm{erf}\left(\frac{1}{2}\sqrt{\xi}\right) - \frac{\vartheta_e}{\mathrm{erf}\left(\frac{1}{2}\sqrt{\xi_e}\right) - 1} \tag{26}$$

In zone $Z2$:

$$\vartheta_2 = \frac{\vartheta_e - 1}{\mathrm{erf}\left(\frac{1}{2}\sqrt{\frac{\kappa_1}{\kappa_2}}\xi_e\right)} \cdot \mathrm{erf}\left(\frac{1}{2}\sqrt{\frac{\kappa_1}{\kappa_2}}\xi\right) + 1 \tag{27}$$

At front $F1$:

Downloaded From: http://heattransfer.asmedigitalcollection.asme.org/ on 06/19/2014 Terms of Use: http://asme.org/terms

$$\frac{4\theta_H K_1}{\rho_h \Delta H \varepsilon_0 \kappa_1}\left(\frac{\vartheta_e \cdot \exp\left(-\frac{1}{4}\xi_e\right)}{2\sqrt{\pi\xi_e}\cdot\left(\operatorname{erf}\left(\frac{1}{2}\sqrt{\xi_e}\right)-1\right)}\right) - \frac{4\theta_H K_2}{\rho_h \Delta H \varepsilon_0 \kappa_1}\left(\sqrt{\frac{\kappa_1}{\kappa_2}}\frac{(\vartheta_e-1)\cdot\exp\left(-\frac{1}{4}\frac{\kappa_1}{\kappa_2}\xi_e\right)}{2\sqrt{\pi\xi_e}\cdot\operatorname{erf}\left(\frac{1}{2}\sqrt{\frac{\kappa_1}{\kappa_2}\xi_e}\right)}\right)=1 \quad (28)$$

If controlling parameters (κ_1/κ_2), (θ_e/θ_H), $(\theta_H K_1/\kappa_1\rho_h\Delta H\varepsilon_0)$, $(\theta_H K_2/\kappa_1\rho_h\Delta H\varepsilon_0)$ are given, ξ_e can be solved from Eq. (28) by a Newtonian iterative method. The expansion of the transformation front can also be expressed as $X_e=\sqrt{\xi_e\kappa_1 t}$. The temperature field can also be obtained.

2.4.2 Two Transformation Fronts Case. For the problem with two transformation fronts, the governing equations and definite conditions in zones $Z1$, $Z2$, and $Z3$ can be rewritten as

In zone Zi (i denote 1, 2, 3 here):

$$4\frac{\mathrm{d}^2\vartheta_i}{\mathrm{d}\xi^2}+\left(\frac{\kappa_1}{\kappa_i}+\frac{2}{\xi}\right)\frac{\mathrm{d}\vartheta_i}{\mathrm{d}\xi}=0 \quad (29)$$

Boundary conditions:

$$\xi\to\infty:\vartheta\to 0;\quad \xi=0:\vartheta=1;\quad \xi=\xi_{e1}:\vartheta=\vartheta_{e1};\quad \xi=\xi_{e2}:\vartheta=\vartheta_{e2} \quad (30)$$

Connecting condition at Fj (j denote 1, 2):

$$\xi=\xi_{ej}:\frac{4\theta_h K_{j+1}}{\rho_h\Delta H\varepsilon_0\kappa_1}\frac{\partial\vartheta_{j+1}}{\partial\xi}-\frac{4\theta_h K_j}{\rho_h\Delta H\varepsilon_0\kappa_1}\frac{\partial\vartheta_j}{\partial\xi}=1 \quad (31)$$

in which, i represents $F1$ or $F2$.

Solutions to Eqs. (29)–(31) are obtained for each zone:

In zone $Z1$:

$$\vartheta_1=\frac{\vartheta_{e2}}{\operatorname{erf}\left(\frac{1}{2}\sqrt{\xi_{e2}}\right)-1}\cdot\operatorname{erf}\left(\frac{1}{2}\sqrt{\xi}\right)-\frac{\vartheta_{e2}}{\operatorname{erf}\left(\frac{1}{2}\sqrt{\xi_{e2}}\right)-1} \quad (32)$$

In zone $Z2$:

$$\vartheta_2=\frac{\vartheta_{e2}-\vartheta_{e1}}{\operatorname{erf}\left(\frac{1}{2}\sqrt{\frac{\kappa_1}{\kappa_2}\xi_{e2}}\right)-\operatorname{erf}\left(\frac{1}{2}\sqrt{\frac{\kappa_1}{\kappa_2}\xi_{e1}}\right)}\cdot\operatorname{erf}\left(\frac{1}{2}\sqrt{\frac{\kappa_1}{\kappa_2}\xi}\right)+\left(\vartheta_{e1}-\frac{\vartheta_{e2}-\vartheta_{e1}}{\operatorname{erf}\left(\frac{1}{2}\sqrt{\frac{\kappa_1}{\kappa_2}\xi_{e2}}\right)-\operatorname{erf}\left(\frac{1}{2}\sqrt{\frac{\kappa_1}{\kappa_2}\xi_{e1}}\right)}\cdot\operatorname{erf}\left(\frac{1}{2}\sqrt{\frac{\kappa_1}{\kappa_2}\xi_{e1}}\right)\right) \quad (33)$$

In zone $Z3$:

$$\vartheta_3=\frac{\vartheta_{e3}-1}{\operatorname{erf}\left(\frac{1}{2}\sqrt{\frac{\kappa_1}{\kappa_3}\xi_{e3}}\right)}\cdot\operatorname{erf}\left(\frac{1}{2}\sqrt{\frac{\kappa_1}{\kappa_3}\xi}\right)+1 \quad (34)$$

Substituting Eqs. (32)–(34) into Eq. (31), ξ_{e1} and ξ_{e2} can be obtained by a Newtonian iterative method, the expansions of transformation fronts $F1$ and $F2$ can be expressed as $X_{e1}=(\xi_{e1}\kappa_1 t)^{1/2}$ and $X_{e2}=(\xi_{e2}\kappa_1 t)^{1/2}$, and the temperature fields can be obtained at the same time.

2.4.3 Three Transformation Fronts Case. For the problem with three transformation fronts, the governing equations and definite conditions in zones $Z1$, $Z2$, $Z3$, and $Z4$ can be rewritten as

In zone Zi (i denote 1, 2, 3, 4):

$$4\frac{\mathrm{d}^2\vartheta_i}{\mathrm{d}\xi^2}+\left(\frac{\kappa_1}{\kappa_i}+\frac{2}{\xi}\right)\frac{\mathrm{d}\vartheta_i}{\mathrm{d}\xi}=0 \quad (35)$$

$$\xi=0:\vartheta=1;\quad \xi\to\infty:\vartheta\to 0;\quad \xi=\xi_{e1}:\vartheta=\vartheta_{e1};\quad \xi=\xi_{e2}:\vartheta=\vartheta_{e2};\quad \xi=\xi_{e3}:\vartheta=\vartheta_{e3} \quad (36)$$

Connecting condition at Fj (j denote 1, 2, 3):

$$\xi=\xi_{ej}:\frac{4\theta_h K_{j+1}}{\rho_h\Delta H\varepsilon_0\kappa_1}\frac{\partial\vartheta_{j+1}}{\partial\xi}-\frac{4\theta_h K_j}{\rho_h\Delta H\varepsilon_0\kappa_1}\frac{\partial\vartheta_j}{\partial\xi}=1 \quad (37)$$

The solutions for each zone are as follows:

In zone $Z1$:

$$\vartheta_1=\frac{\vartheta_{e2}}{\operatorname{erf}\left(\frac{1}{2}\sqrt{\xi_{e2}}\right)-1}\cdot\operatorname{erf}\left(\frac{1}{2}\sqrt{\xi}\right)-\frac{\vartheta_{e2}}{\operatorname{erf}\left(\frac{1}{2}\sqrt{\xi_{e2}}\right)-1} \quad (38)$$

In zone $Z2$:

$$\vartheta_2=\frac{\vartheta_{e2}-\vartheta_{e1}}{\operatorname{erf}\left(\frac{1}{2}\sqrt{\frac{\kappa_1}{\kappa_2}\xi_{e2}}\right)-\operatorname{erf}\left(\frac{1}{2}\sqrt{\frac{\kappa_1}{\kappa_2}\xi_{e1}}\right)}\cdot\operatorname{erf}\left(\frac{1}{2}\sqrt{\frac{\kappa_1}{\kappa_2}\xi}\right)+\left(\vartheta_{e1}-\frac{\vartheta_{e2}-\vartheta_{e1}}{\operatorname{erf}\left(\frac{1}{2}\sqrt{\frac{\kappa_1}{\kappa_2}\xi_{e2}}\right)-\operatorname{erf}\left(\frac{1}{2}\sqrt{\frac{\kappa_1}{\kappa_2}\xi_{e1}}\right)}\cdot\operatorname{erf}\left(\frac{1}{2}\sqrt{\frac{\kappa_1}{\kappa_2}\xi_{e1}}\right)\right) \quad (39)$$

In zone $Z3$:

$$\vartheta_3=\frac{\vartheta_{e3}-\vartheta_{e2}}{\operatorname{erf}\left(\frac{1}{2}\sqrt{\frac{\kappa_1}{\kappa_3}\xi_{e3}}\right)-\operatorname{erf}\left(\frac{1}{2}\sqrt{\frac{\kappa_1}{\kappa_3}\xi_{e2}}\right)}\cdot\operatorname{erf}\left(\frac{1}{2}\sqrt{\frac{\kappa_1}{\kappa_3}\xi}\right)+\left(\vartheta_{e2}-\frac{\vartheta_{e3}-\vartheta_{e2}}{\operatorname{erf}\left(\frac{1}{2}\sqrt{\frac{\kappa_1}{\kappa_3}\xi_{e3}}\right)-\operatorname{erf}\left(\frac{1}{2}\sqrt{\frac{\kappa_1}{\kappa_3}\xi_{e2}}\right)}\cdot\operatorname{erf}\left(\frac{1}{2}\sqrt{\frac{\kappa_1}{\kappa_3}\xi_{e2}}\right)\right) \quad (40)$$

In zone $Z4$:

$$\vartheta_4=\frac{\vartheta_{e4}-1}{\operatorname{erf}\left(\frac{1}{2}\sqrt{\frac{\kappa_1}{\kappa_4}\xi_{e4}}\right)}\cdot\operatorname{erf}\left(\frac{1}{2}\sqrt{\frac{\kappa_1}{\kappa_4}\xi}\right)+1 \quad (41)$$

Substituting Eqs. (38)–(41) into Eq. (37), ξ_{e1}, ξ_{e2}, and ξ_{e3} can be obtained by a Newtonian iterative method, the expansions of transformation fronts $F1$, $F2$, and $F3$ can be expressed as

Downloaded From: http://heattransfer.asmedigitalcollection.asme.org/ on 06/19/2014 Terms of Use: http://asme.org/terms

$X_{e1}=(\xi_{e1}\kappa_1 t)^{1/2}$, $X_{e2}=(\xi_{e2}\kappa_1 t)^{1/2}$, and $X_{e3}=(\xi_{e3}\kappa_1 t)^{1/2}$, and the temperature fields can be obtained using the obtained parameters.

2.5 Numerical Simulation. A numerical method is proposed here to analyze the evolution of phase transformation fronts in HBS with a finite length. The numerical solutions can be compared with the analytical solutions.

The dimensionless governing equation, boundary and initial conditions in Eqs. (8)–(11) can be expressed using three basic units, i.e., experimental length l, hydrate dissociation temperature T_{eh}, and thermal diffusivity of soil skeleton $K_s/\rho_s C_s$.

Governing equation:

$$\frac{\partial T}{\partial t}=a^2\frac{\partial^2 T}{\partial x^2},\quad a^2=\frac{\rho_s C_s}{K_s}\frac{K}{\rho C} \tag{42}$$

Boundary condition:

$$x=0,\quad T=\frac{T_H}{T_{eh}}\quad\text{and}\quad x=1,\quad T=\frac{T_0}{T_{eh}} \tag{43}$$

Initial condition:

$$t=0,\quad T=\frac{T_0}{T_{eh}} \tag{44}$$

Connecting condition at the fronts:

$$T(X_{ei}(t))=\frac{T_{ei}}{T_{eh}},\quad \left.\frac{\partial T}{\partial x}\right|_{X_{ei}+}-\left.\frac{\partial T}{\partial x}\right|_{X_{ei}-}=\frac{\rho_i\Delta H\varepsilon_i}{\rho C T_{eh}}\frac{\mathrm{d}X_{ei}}{\mathrm{d}t} \tag{45}$$

Equations (42)–(45) are discretized using the Crank-Nicolson difference method.

Governing equation:

$$\frac{T_j^{n+1}-T_j^n}{\Delta t}=\frac{a^2}{2\Delta h^2}\left[(T_{j+1}^{n+1}-2T_j^{n+1}+T_{j-1}^{n+1})+T_{j+1}^n-2T_j^n+T_{j-1}^n\right]\times j=1,2,\ldots,N \tag{46}$$

Boundary condition:

$$T_0^n=T_H,\quad T_N^n=T_{N-1}^n \tag{47}$$

Initial condition:

$$T^0=\frac{T_0}{T_{eh}} \tag{48}$$

If the temperature at location j reaches T_{ei}/T_{eh}, phase transformation will occur, and the temperature keeps constant until the input heat equals the enthalpy of hydrate dissociation, i.e.,

$$\sum_n^{n+m}\left(\frac{T_{j-1}^n-T_j^n}{\Delta x}-\frac{T_j^n-T_{j+1}^n}{\Delta x}\right)\Delta t=\frac{\rho_i\Delta H\varepsilon_i}{\rho C T_{e1}}\Delta h \tag{49}$$

After a duration of $m\cdot\Delta t$, the transformation process at j is finished, and the temperature at $j+1$ will reach T_{ei}/T_{eh}. Phase transformation will occur at $j+1$ and the temperature will reach T_{ei}/T_{eh} at $j+2$ until the input heat equals the enthalpy of hydrate dissociation at $j+1$. Here, superscripts n and m indicate time steps; subscripts i and j indicate space coordinates.

In addition, the density of gas at the maximum pressure, 0.1 MPa in the experiments to be reported later is adopted in the numerical simulation. The specific heat of gas is determined by $C=3R/M$. The heat conduction coefficient is assumed to be the same as that of water vapor though it changes with temperature. Analysis shows that these approximations have little influence on the evolution of phase transformation fronts due to small gas volume fraction.

3 Experimental Verification

3.1 Measurement Techniques

3.1.1 Apparatus. To obtain parameters for one-dimensional theoretical analysis, experiments have been conducted in a plexiglass cylinder 100 mm in diameter and 300 mm in height. With the one dimensional experimental set-up, the boundary conditions can be controlled and the experimental results can be applied to verify the theoretical analysis. In this model, an immersion heater with a power of 400 W and a diameter of 80 mm is horizontally placed at the bottom of the plexiglass cylinder as a heat source, and a diameter of 100 mm and a height of 20 mm ceramic plate is placed under the heat source as a heat insulator. A liquid or gas inlet is set at the bottom of the cylinder to saturate the sediment. Several scales are marked at the external surface of the cylinder, and a camera is used to record the expansion of the transformation fronts (Fig. 4), and temperature sensors are placed above the heat source at an interval of 2 cm to measure the temperature at the mid of the sediment when the transformation fronts arrive.

3.1.2 Experimental Procedure. The experimental procedure is as follows:

(1) A thermal source with a temperature regulator and several temperature sensors are placed at the designated location. A silty sand with a dry density of 1.6 g/cm^3 was first compacted to a height of 250 mm as the skeleton.
(2) The skeleton was saturated from the bottom to the top by THF-water mixture with a mass fraction of 19% THF through an inlet. The cylinder was placed in a refrigerator for 3–5 days at a temperature of −8 °C to assure full formation of THF hydrate sediment (the temperature kept at about 4 °C for more than 6 h).
(3) The maximum output temperature of the heater was controlled by a temperature regulator. The outside of the cylinder was wrapped (But the scales were left visible) by thermal insulation materials to reduce the heat diffusion. Then the heater, video recorder and sensors were turned on. During the experiments, the environmental temperature was kept at −8 °C.
(4) HBS was heated under a constant designated temperature. When the phase transformation fronts (The temperature is about 4.4 °C at this moment) arrived at a temperature sensor, the temperature of phase transformation and the time were recorded. The evolution of phase transformation fronts during hydrate dissociation was observed by referring to the scales in the video and readings of the temperature sensors.

3.1.3 Experimental Conditions. The critical temperatures of phase transformations from THF hydrate to THF liquid and water,

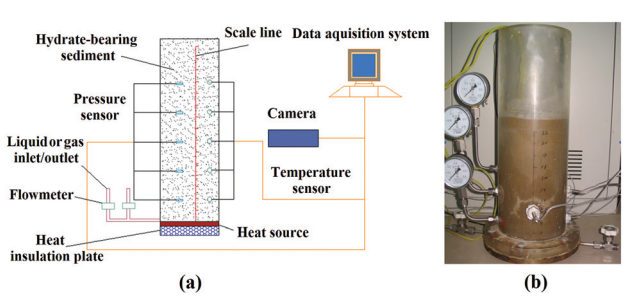

Fig. 4 Layout of one-dimensional cylinder. (*a*) Schematic diagram. (*b*) Photo of the one-dimensional cylinder.

Downloaded From: http://heattransfer.asmedigitalcollection.asme.org/ on 06/19/2014 Terms of Use: http://asme.org/terms

Table 1 Thermal conduction parameters [27]

Label	Parameter	Sign and value	Label	Parameter	Sign and value
1	Initial temperature	$T_0 = 265.15$ (K)	18	Specific heat of water	$C_w = 4211$ (J/kg K)
2	Density of sand grain	$\rho_s = 2650$ (kg/m^3)	19	Specific heat of THF gas	$C_{fg} = 346$ (J/kg K)
3	Fraction of sediment skeleton	$\varepsilon_s = 0.6$	20	Specific heat of sand skeleton	$C_s = 840$ (J/kg K)
4	Fraction of hydrate	$\varepsilon_h = 0.4$	21	Specific heat of THF	$C_f = 1960$ (J/kg K)
5	Length of experimental zone	$l = 0.25$ (m)	22	Thermal conduction coefficient of water vapor	$K_{wg} = 0.03$ (W/m K)
6	Density of THF hydrate	$\rho_h = 997$ (kg/m^3)	23	Thermal conduction coefficient of THF gas	$K_{fg} = 0.03$ (W/m K)
7	Thermal conduction coefficient of THF hydrate	$K_h = 0.46$ (W/m K)	24	Thermal conduction coefficient of water	$K_w = 0.56$ (W/m K)
8	Enthalpy of THF hydrate dissociation	$\Delta H_{h\to f} = 2.7 \times 10^5$ (J/K)	25	Thermal conduction coefficient of sand skeleton	$K_s = 3$ (W/m K)
9	Phase equilibrium temperature of THF hydrate	$T_{eh} = 277.15$ (K)	26	Thermal conduction coefficient of THF	$K_f = 0.12$ (W/m K)
10	Specific heat of THF hydrate	$C_h = 2123$ (J/kg/K)	27	Points of difference grid	$N = 100$
11	Enthalpy of THF gasification	$\Delta H_{f\to fg} = 4.1 \times 10^5$ (J/K)	28	Thermal diffusion coefficient	$K_s/\rho_s C_s = 10^{-7}$ (m/s)
12	Density of THF	$\rho_f = 890$ (kg/m^3)	29	Gas cohesion coefficient	$\mu_g = 10^{-5}$ (Pa·s)
13	Gasification temperature of THF	$T_{ef} = 339.15$ (K)	30	Permeability of sediments	$k_g = 10^{-15}$ (m^2)
14	Vaporization of water	$T_{ew} = 373.15$ (K)	31	Elastic modulus of sediments	$E = 500$ (MPa)
15	Density of water	$\rho_w = 1000$ (kg/m^3)	32	Equilibrium pressure	$p_e = 10$ (MPa)
16	Enthalpy of water vaporization	$\Delta H_{w\to wg} = 2.2 \times 10^6$ (J/K)	33	Time step	$\Delta t = 10^{-4}$
17	Specific heat of steam	$C_{wg} = 1385$ (J/kg K)	34	Spatial step	$\Delta h = 10^{-2}$

Table 2 Different temperature conditions

Temperature condition (referred to Fig. 1)	Z4	F3	Z3	F2	Z2	F1	Z1
110, 150, 200, and 300 °C	Yes	Yes	Yes	Yes	Yes	Yes	Yes
80 °C	—	—	Yes	Yes	Yes	Yes	Yes
50 °C	—	—	—	—	Yes	Yes	Yes

THF liquid to THF gas and water to vapor are 4.4, 66, and 100 °C, respectively. So the experiments were conducted at six temperatures of 50, 80, 110, 150, 200, and 300 °C to simulate three different kinds of evolution of phase transformation fronts.

3.2 Comparison of Experimental, Analytical, and Numerical Results. Theoretical analysis and numerical simulations of the evolution of different phase transformation fronts and zones involved in the experiments in Table 1 were conducted. Six temperatures were considered. The input parameters are shown in Table 2, which are the same as those involved in the experiments.

The results of the experimental, analytical and numerical studies on the evolution of hydrate dissociation fronts at temperatures of 50, 80, 110, 150, 200, and 300 °C were compared.

Several observations can be made:

(1) At a temperature of 50 °C, a phase transformation front F1 occurred and expanded. Then two zones $Z1$ and $Z2$ formed. The expansion of the transformation front $F1$ was measured using both the temperature sensors and the scales in the experiments. The observed phase transformation front of hydrate dissociation expanded as a horizontal cross section and the measured temperature in the mid of the front was about 4.4 °C (the temperature of THF hydrate phase transformation), i.e., the temperature in the cross section was uniform and one dimension condition could be considered to apply approximately. The experimental, analytical, and numerical results are in good agreement (Fig. 5). The small differences may be caused mainly by the artificial selection of integral time point for plotting in numerical studies.

(2) At a temperature of 80 °C, two phase transformation fronts $F1$ and $F2$ occurred and expanded, then three zones $Z1$, $Z2$, and $Z3$ formed. The expansion of the transformation front $F1$ was measured by the temperature sensors in the experiment, but the expansion of the transformation front $F2$ was not obtained because the color difference between $Z2$ and $Z3$ could not be distinguished clearly as $Z2$ and $Z3$ shared the same compositions of water and sediment skeleton, meanwhile the transformation front $F2$ moved too

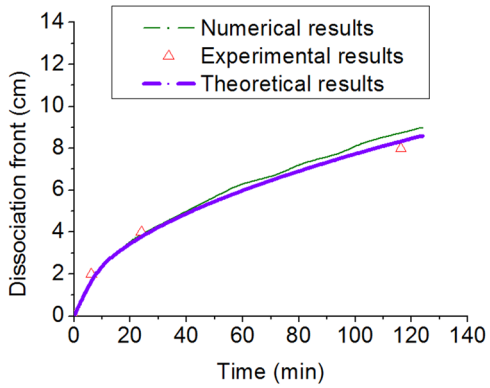

Fig. 5 Comparison of experimental, analytical, and numerical results for the hydrate to THF and water transformation front in a one-front experiment

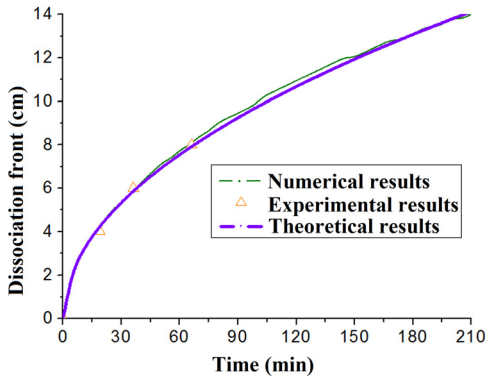

Fig. 6 Comparison of experimental, analytical, and numerical results for the hydrate to THF and water transformation front in a two-front experiment

Downloaded From: http://heattransfer.asmedigitalcollection.asme.org/ on 06/19/2014 Terms of Use: http://asme.org/terms

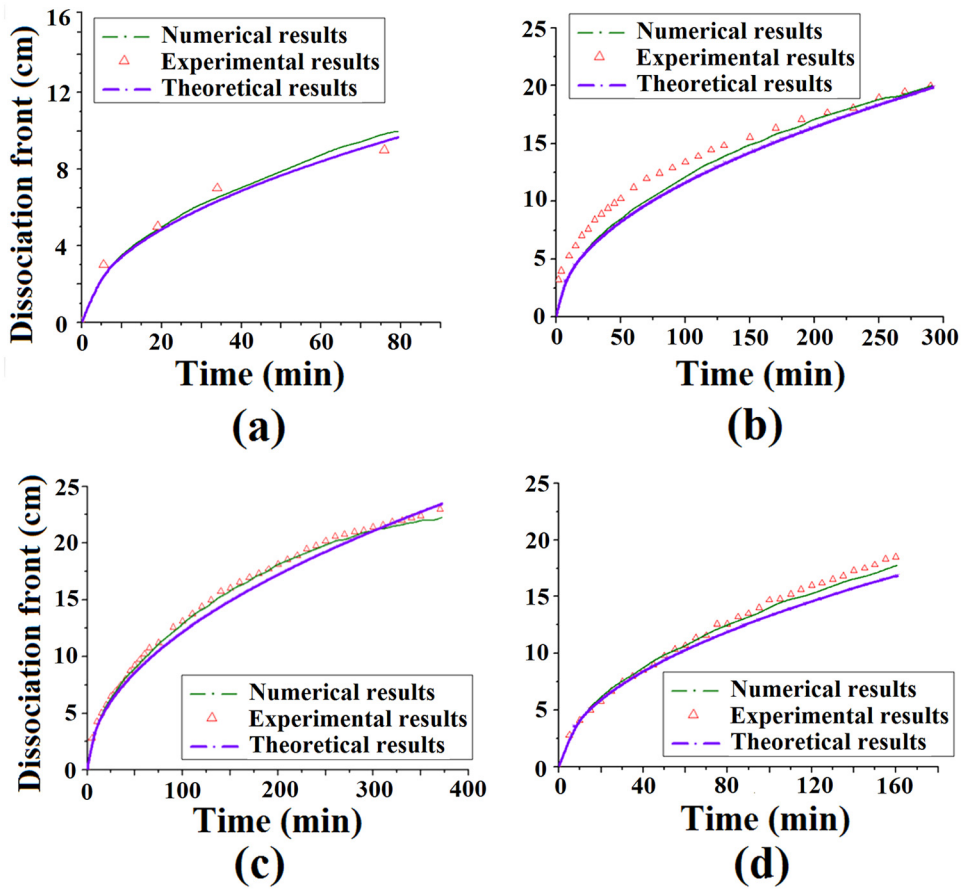

Fig. 7 Comparison of experimental, analytical and numerical results for the hydrate to THF and water transformation front in a three-front experiment. (*a*) Heating temperature = 110 °C. (*b*) Heating temperature = 150 °C. (*c*) Heating temperature 200 °C. (*d*) Heating temperature 300 °C.

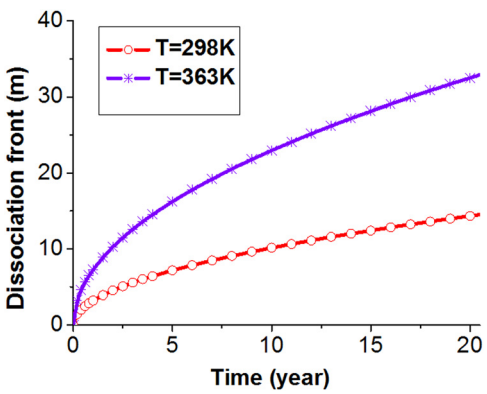

Fig. 8 Evaluations for exploitation of gas hydrate

slowly to be measured by temperature sensors. The experimental, analytical and numerical results are in good agreement in this case (Fig. 6).

(3) At temperatures of 110 °C, 150 °C, 200 °C, and 300 °C, three-phase transformation fronts $F1$, $F2$, and $F3$ could be observed, and four zones $Z1$, $Z2$, $Z3$, and $Z4$ formed. The expansion of the transformation front $F1$ could be measured by temperature sensors and the scales in the experiment, but the expansion of the transformation front F3 could not be obtained because it expanded very slowly. Figure 7 shows the experimental, analytical, and numerical results.

(4) Thermal simulations based on our model and the data for thermal properties of methane hydrate sediments in the Shenhu area of South China Sea [33] are conducted. The results shown in Fig. 8 are that the dissociation front expands 15 m and 33 m after 20 years when the heating temperature is 298 K (for surface seawater injection) and 363 K (for steam injection), respectively. The fully hydrate dissociated zone is 4 m similar to that of the TOUGH + HYDRATE simulation (About 4.5 m, [33]), and the reason of the difference may be that the seepage and the different expression of thermal conductivity were considered in the TOUGH + HYDRATE simulation. Here we can note that the thermal simulation is ineffective, and new hydrate recovery methods are required for exploration and utilization of natural gas hydrate sediments.

4 Conclusions

A new model is proposed to describe the thermal conduction considering one-, two-, and three-phase transformation fronts. A method of self-similarity is presented and analytic solutions to the governing equations are obtained. Laboratory experiments in six temperature conditions are conducted using THF HBS in a one-dimensional cylinder to verify the new model and its solutions.

The following conclusions are drawn:

(1) The physical process of the evolution of hydrate dissociation can be described as follows: (a) heat transfer leads to hydrate dissociation and phase transformations; (b) phase transformation expands as fronts and different zones form divided by the fronts.

(2) The evolution of hydrate dissociation and phase transformation fronts is self-similar.

(3) The analytical results illustrate that the expansion of hydrate dissociation and the phase transformation fronts in the sediments is proportional to the square root of time.

Downloaded From: http://heattransfer.asmedigitalcollection.asme.org/ on 06/19/2014 Terms of Use: http://asme.org/terms

(4) The experimental, analytical and numerical results of expansion of the hydrate dissociation front are in good agreement.
(5) The thermal conductivity of THF hydrate sediments can be expressed as average that of each composition.
(6) The dissociation front expands so slow that new methods should be considered to improve the recovery of gas hydrate except depressurization and thermal simulation.

It should be noted only a hydrate dissociation front is measured experimentally, and the development of gas seepage in the sediment is ignored in the present model. The seepage of released gas and water and the redistribution of pore pressure and stresses in the sediment should be considered in the future.

Acknowledgment

This study is supported by the National Natural Science Foundation of China (NSFC) (Nos. 11102209 and 51239010).

Nomenclature

C = specific heat
f = liquid
$f \rightarrow fg$ = phase transformations from liquid to gas
F = phase transformation front
fg = gas THF
h = hydrate
$h \rightarrow w+f$ = phase transformations from hydrate to water and liquid
$H(x)$ = Heaviside function, i.e., $x \geq 0, H(x) = 1; x < 0, H(x) = 0$
κ = thermal diffusivity
K = thermal conductivity
M = mole mass
R = gas constant
s = sediment
t = time
T = temperature
T_{eh} = hydrate phase transformation temperature
T_H = heating temperature
T_0 = initial temperature
w = water
$w \rightarrow wg$ = phase transformations from water to water vapor
wg = water vapor
x = spatial position
X_{ef} = the positions of phase transformation fronts of liquid THF
X_{eh} = the positions of phase transformation fronts of hydrate
X_{ew} = the positions of phase transformation fronts of water
$\mathbf{Z}$ = zone
ΔH = Enthalpy
Δh = spatial step
Δt = time step
ε = volume fraction
ε_0 = porosity of sediment
θ = temperature difference to initial temperature
ξ = self-similarity variable
ρ = Density
ϑ = dimensionless temperature
ϑ_e = dimensionless phase transformation temperature

References

[1] Sloan, E. D., 1998, *Clathrate Hydrates of Natural Gases*, Marcel Dekker Inc., New York.
[2] Guerin, G., Goldberg, D., and Melser, A., 1999, "Characterization of In-Situ Elastic Properties of Gas Hydrate Bearing Sediments on the Blake Ridge," J. Geophys. Res., **104**(B8), pp. 17781–17795.
[3] Kvenvolden, K. A., and Lorenson, T. D., 2001, "The Global Occurrence of Natural Gas Hydrate," Geophy. Monog. Ser., **124**, pp. 3–18.
[4] Riedel, M., Bellefleur, G., Dallimore, S., Taylor, A., and Wright, J., 2006, "Amplitude and Frequency Anomalies in Regional 3D Seismic Data Surrounding the Mallik 5L-38 Research Site, Mackenzie Delta, Northwest Territories, Canada," Geophysics, **71**(6), pp. B183–B191.
[5] Bouriak, S., Vanneste, M., and Soutkine, A., 2000, "Inferred Gas Hydrates and Clay Diapers Near the Storegga Slide on the Southern Edge of the Vφring Plateau, Off Shore Norway," Mar. Geol., **163**, pp. 125–148.
[6] Driscoll, N. W., Weissel, J. K., and Goff, J. A., 2000, "Potential for Large Scale Submarine Slope Failure and Tsunami Generation Along the US Mid-Atlantic Coast," Geology, **28**(5), pp. 407–410.
[7] Jung, W. Y., and Vogt, P. V., 2004, "Effects of Bottom Water Warming and Sea Level Rise on Holocene Hydrate Dissociation and Mass Wasting Along the Norwegian-Barents Continental Margin," J. Geophy. Res., **109**(B6), pp. B06104.1–B06104.18.
[8] Milkov, A. V., 2000, "Worldwide Distribution of Submarine Mud Volcanoes and Associated Gas Hydrates," Mar. Geol., **167**, pp. 29–42.
[9] Sultan, N., Cochonat, P., Foucher, J. P., and Mienert, J., 2004, "Effect of Gas Hydrates Melting on Seafloor Slope Instability," Mar. Geol., **213**(1–4), pp. 379–401.
[10] Xu, W., and Germanovich, L. N., 2006, "Excess Pore Pressure Resulting from Methane Hydrate Dissociation in Marine Sediments: A Theoretical Approach," J. Geophys. Res., **111**, p. 011104.
[11] Kwon, T. H., Cho, G. C., and Santamarina, J. C., 2008, "Gas Hydrate Dissociation in Sediments: Pressure-Temperature Evolution," Geochem. Geophys. Geosyst., **9**(3), p. Q03019.
[12] Waite, W. F., Kneafsey, T. J., Winters, W. J., and Mason, D. H., 2008, "Physical Property Changes in Hydrate-Bearing Sediment due to Depressurization and Subsequent Repressurization," J. Geophys. Res., **113**, p. B07102.
[13] Zhang, X. H., Lu, X. B., and Li, Q. P., 2010, "Formation of Layered Fracture and Outburst During Gas Hydrate Dissociation," J. Petrol. Sci. Eng., **76**(3–4), pp. 212–216.
[14] Gong, Y. M., Indrakanti, V. P., Perez, P. L., Powers, S., and Venkataraman, R., 2004, "Offshore Methane Hydrates: Optimal Recovery and Utilization," EGEE 580/FSc 503, Final Report Team II, pp. 1–52.
[15] Briaud, J. L., and Chaouch, A. J., 1997, "Hydrate Melting in Hydrate Soil Around Hot Conductor," J. Geotech. Geoeng. Eng., **123**(7), pp. 645–653.
[16] Makogon, Y. F., 1997, *Hydrates of Hydrocarbons*, Penn Well, Tulsa, OK.
[17] Ji, C., Ahmadi, G., and Smith, G. H., 2001, "Natural Gas Production from Hydrate Decomposition by Depressurization," Chem. Eng. Sci., **56**, pp. 5801–5814.
[18] Moridis, G. J., Collett, T. S., Boswell, R., Kurihara, M., Reagan, M. T., Koh, C., and Sloan, E. D., 2009, "Toward Production from Gas Hydrates: Current Status, Assessment of Resources, and Simulation-Based Evaluation of Technology and Potential," SPE Res. Eva. Eng., **12**(5), pp. 745–771.
[19] Kimoto, S., Oka, F., and Fushita, T., 2010, "A Chemo-Thermo-Mechanically Coupled Analysis of Ground Deformation Induced by Gas Hydrate Dissociation," Int. J. Mech. Sci., **52**(2), pp. 365–376.
[20] Klar, A., Soga, K., and Ng, M. Y. A., 2010, "Coupled Deformation-Flow Analysis for Methane Hydrate Extraction," Geotechnique, **60**(10), pp. 765–776.
[21] Gerami, S., and Pooladi-Darvish, M., 2007, "Predicting Gas Generation by Depressurization of Gas Hydrates Where the Sharp-Interface Assumption is Not Valid," J. Petrol. Sci. Eng., **56**(1–3), pp. 146–164.
[22] Tohidi, B., Anderson, R., Clennell, M. B., Burgass, R. W., and Biderkab, A. B., 2001, "Visual Observation of Gas Hydrate Formation and Dissociation in Synthetic Porous Media by Means of Glass Micromodels," Geology, **29**(9), pp. 867–870.
[23] Jones, K. W., Kerkar, P. B., Mahajan, D., Lindquist, W. B., and Feng, H., 2007, "Microstructure of Natural Hydrate Host Sediments," Nucl. Instrum. Methods Phys. Res. B, **261**(1–2), pp. 504–507.
[24] Koh, C. A., 2002, "Towards a Fundamental Understanding of Natural Gas Hydrates," Chem. Soc. Rev., **31**(3), pp. 157–167.
[25] Yun, T. S., Santamarina, J. C., and Ruppel, C., 2007, "Mechanical Properties of Sand, Silt, and Clay Containing Tetrahydrofuran Hydrate," J. Geophys. Res., **112**, p. B04106.
[26] Lee, J. Y., Yun, T. S., Santamarina, J. C., and Ruppel, C., 2007, "Observations Related to Tetrahydrofuran and Methane Hydrates for Laboratory Studies of Hydrate-Bearing Sediments," Geochem. Geophys. Geosyst., **8**(6), p. Q06003.
[27] Zhang, X. H., Lu, X. B., Li, Q. P., and Yao, H. Y., 2010, "Thermally Induced Evolution of Phase Transformations in Gas Hydrate Sediment," Sci. China Phys., Mech. Astro., **53**(8), pp. 1530–1535.
[28] OZisik, M. N., 1980, *Heat Conduction*, John Wiley, New York.
[29] Cortes, D. D., Martin, A. I., Yun, T. S., Francisca, F. M., Santamarina, J. C., and Ruppel, C., 2009, "Thermal Conductivity of Hydrate-Bearing Sediments," J. Geophys. Res., **114**, p. B11103.
[30] Waite, W. F., Santamarina, J. C., Cortes, D. D., Dugan, B., Espinoza, D. N., Germaine, J., Jang, J., Jung, J. W., Kneafsey, T. J., Shin, H., Soga, K., Winters, W. J., and Yun, T. S., 2009, "Physical Properties of Hydrate-Bearing Sediments," Rev. Geophys., **47**, pp. 1–38.
[31] Lee, J. Y., Ryu, B. J., Yun, T. S., Lee, J., and Cho, G. C., 2011, "Review on the Gas Hydrate Development and Production as a New Energy Resource," KSCE J. Civ. Eng., **15**(4), pp. 689–696.
[32] Cannon, J. R., and Hill, C. D., 1967, "Existence, Uniqueness, Stability and Monotone Dependence in a Stefan Problem for the Heat Equation," J. Math. Mech., **17**, pp. 1–19.
[33] Li, G., Moridis, G. J., Zhang, K. N., and Li, X. S., 2011, "The Use of Huff and Puff Method in a Single Horizontal Well in Gas Production From Marine Hydrate Deposits in Shenhu Area of South China Sea," J. Petrol. Sci. Eng., **77**(1), pp. 49–68.

Downloaded From: http://heattransfer.asmedigitalcollection.asme.org/ on 06/19/2014 Terms of Use: http://asme.org/terms